Engineering Technology Open Access Journal

Juniper Publishers key to the Researchers

Research article
Volume 5 Issue 5 - January 2024
DOI: 10.19080/ETOAJ.2024.05.555671

Eng Technol Open Acc

Study of Thermal Insulation Nature of $A_2Fe_2O_{6-\delta}$ (A and A' = Ca, Sr)

Ram Krishna Hona[1*], Amara Martinson[1], Mandy Guinn[1] and Alexa D Azure[2]

[1]*Environmental Science Department, United Tribes Technical College, Bismarck, ND 58504, USA*

[2]*Engineering Department, United Tribes Technical College, Bismarck, ND 58504, USA*

Submission: December 12, 2023; **Published:** January 9, 2024

***Corresponding author:** Ram Krishna Hona, Environmental Science Department, United Tribes Technical College, Bismarck, ND 58504, USA, Email: rhona@uttc.edu

Abstract

Materials with low thermal conductivity have been used in thermoelectrics, electronics, solar devices, and land base and aerospace gas turbines to prevent heat dissipation and provide safety and longevity of equipment. We report $Ca_2Fe_2O_{6-\delta}$, and $Sr_2Fe_2O_{6-\delta}$ for their low thermal conductivities. These compounds are vacancy-ordered oxygen-deficient perovskites but with different vacancy arrangements. $Ca_2Fe_2O_{6-\delta}$ has a brownmillerite type structure while $Sr_2Fe_2O_{6-\delta}$ has a different structure. $Ca_2Fe_2O_{6-\delta}$, and $Sr_2Fe_2O_{6-\delta}$, both exhibit low thermal conductivity of less than $1Wm^{-1}K^{-1}$ which is among the lower values of the recently reported perovskite materials. The reason for the low thermal conductivity is attributed to the oxygen vacancy and phonon scattering. Since the reported perovskite oxides with high thermal conductivity are structurally disordered, the low thermal conductivity may be attributed to the structural order of the materials.

Keywords: Thermal Insulation; Perovskite Structure; Thermoelectrics

Introduction

Since thermal insulation provides safety and longevity to heat-based equipment such as the turbines and blades of airplanes and aerospace, research has been undergoing intensively to reduce the thermal conductivity of possible materials. For example, titanate-based ceramics, [1] composite materials, [2] zirconia, and yttria-based materials, [3] etc. have been under study for low thermal conductivity. Materials with low thermal conductivity have applications in thermoelectrics as well [4,5] Different classes of materials such as perovskite oxides, pyrochlore, [1] nanophase [6], and Zintl phases of intermetallics [7] have been studied for low thermal conductivity. Similarly, different methods and principles have been applied to reduce thermal conductivity. For example, coating, alloy formation, introduction of twin interface [8], etc. are different methods employed to reduce the thermal conductivity. Since ceramics have a high melting point, ceramic-based oxides are more attractive. One of the highly attractive ceramic-based oxides for thermal insulation include perovskite oxides [4].

Perovskite oxides are represented by a general formula of ABO_3 where A and B represent alkaline earth or rare earth metal and transition metal, respectively. An ideal perovskite oxide exhibits a cubic structure with A cations surrounded by BO_6 octahedra, B cations at the center of octahedra, and O anions at the corners of the octahedra. The reduction of thermal conductivity of perovskite oxides has been practiced by different methods such as generation of oxygen vacancy in the crystal lattice of the materials, lattice distortions, grain size reduction, grain boundary introduction or randomization, etc. However, oxygen vacancy generation has been found more effective for the reduction of thermal conductivity in perovskite oxides. Oxygen-deficient perovskites are expressed as ABO_{3-x} or $A_2B_2O_{6-\delta}$. Where x and δ represent oxygen vacancy concentration. Since the vacancies can have a large possibility of distribution such as concentration and order type, oxygen vacancies (or oxygen defects) in ODPs bring about structural flexibility in them giving rise to the possibility of different structures. Thus, the vacancy can be ordered or disordered in the crystal system. The vacancy disordered ODP can resemble the cubic system of a fully occupied parent perovskite structure. When the vacancy arrangement is ordered, several ways of arrangements can be found resulting in different structures. In vacancy-ordered materials, the vacancy may form tetrahedra or square pyramids like various coordination geometries around B cations in the crystal system [9]. Oxygen vacancy can be generated in perovskite oxides by reductions or preparing the materials in reducing environments. For example, $CaMnO_3$ is a cubic perovskite that can be reduced to $CaMnO_{2.5}$ by reduction or it is prepared under a reducing environment [10]. Similarly, $SrMnO_3$ can also be

reduced to $SrMnO_{2.6}$ and $SrMnO_{2.5}$ or they are prepared in reducing environments [11]. The oxygen vacancy can also be generated by A or B cation substitution. This substitution can change the concentration of the vacancy or the ordering type of the vacancies.

Though there are various contributions to the thermal conductivity of polycrystalline perovskite oxide, the thermal conductivity, in general, dominantly takes place through phonons and charge carriers. When phonons are dominant factors, the thermal conductivity of such materials can be reduced by increasing phonon scattering. The thermal conductivity of a material decreases with the increase of phonon scattering because the heat flow takes place through a spectrum of phonons with different wavelengths and mean free paths [12,13] and the interference on thermal phonons slows the propagation of heat. Phonon scattering can be increased by different ways such as vacancy generation, impurity introduction, lattice distortion, grain size reduction, grain boundary introduction or randomization, etc. Oxygen vacancies can sometimes have a dominant impact over other contributions in increasing phonon scattering and lowering thermal conductivity.

Vacancy generation can also lead to the transformation of the crystal structure as in the reduction of $CaMnO_3$ and $SrMnO_3$. The enhancement of the thermal insulation property by vacancy generation is not surprising because there are examples of other functional properties that have been improved by the generation of oxygen vacancy along with structural transformation. In the case of $CaMnO_3$ and $SrMnO_3$, the generation of oxygen vacancy transforms their crystal structure to different ones of $CaMnO_{2.5}$, $SrMnO_{2.5}$, and $SrMnO_{2.6}$ improving the electrocatalytic activity toward oxygen evolution reactions [10,11]. Similarly, greater oxygen vacancy concentration brought about by A cation substitution can lead to phonon scattering enhancement and thermal conductivity reduction. One example of the improvement of thermal insulation property by oxygen vacancy increment can be discussed in the materials $Sr_2FeCoO_{6-\delta}$ and $Ca_2FeCoO_{6-\delta}$ [14]. When Sr_2 is substituted by Ca_2, the resulting material $Ca_2FeCoO_{6-\delta}$ with higher vacancy concentration exhibits higher thermal insulation. An attempt to generate vacancy was accomplished through A site cation substitution to reduce the thermal conductivity in $La_{1-x}Ba_xCoO_3$ (x= 0.01,0.03 and 0.05). The thermal conductivity was reduced to 0.5-0.6 $Wm^{-1}K^{-1}$ [15,16]. The role of oxygen vacancy in reducing thermal conductivity was illustrated in $BaSnO_3$ [17]. Oxygen vacancy creation to reduce the thermal conductivity was studied on other classes of oxide materials also [18]. Thus, vacancy generation can lead to lower thermal conductivity.

Though there are attempts to generate oxygen vacancy to lower the thermal conductivity of perovskite oxides, [16,19] attention has not been found on vacancy ordered or layered oxide materials for thermal insulation properties. Here in this article, we report the low thermal conductivity, or high thermal insulation property of vacancy-ordered ODPs such as $Ca_2Fe_2O_{6-\delta}$, and $Sr_2Fe_2O_{6-\delta}$ for which the thermal conductivities were investigated using a Thermtest thermal conductivity meter, MP-2 with TPS-4. The detailed method is described in the supporting information.

Experimental

$SrCO_3$, $CaCO_3$, Co_3O_4 and Fe_2O_3 powders were used for the synthesis of $Ca_2Fe_2O_{6-\delta}$, and $Sr_2Fe_2O_{6-\delta}$. The powders were weighed and mixed uniformly in stoichiometric proportion using agate mortar and a pestle. Pellets were prepared from the powders at a pressure of 3 tons and calcined at 1000 ^{0}C for 24 hours. The pellets were cooled down to room temperature to regrind and re-pelletize. The pellets were sintered at 1200 ^{0}C for 24 hours. The heating rate for calcination and sintering was 100 °C/h. The samples were tested for their crystal structure and phase purity through the help of powder X-ray diffraction (PXRD) with Cu Kα1 and Kα2 radiations of wavelength, λ = 1.54056 Å. GSAS software [20] (Larson and Von Dreele 1994) and EXPEGUI interface [21] (Toby 2001) was used for Rietveld refinements of the XRD data. The scanning micrographs of the materials were investigated for their microstructures study. The concentration of oxygen vacancy of the materials was determined by iodometric titrations. For this, 2 g of potassium iodide was mixed with 50 mg of a sample in 100 mL of 1M HCl. 5 mL of the solution was transferred into a conical flask and then 25 mL of water was added to it to increase the volume. It is titrated against 0.025 M $Na_2S_2O_3$. 0.2 mL of a starch solution was added as an indicator near the end of the titration. The whole experiment was performed under an argon atmosphere. The thermal conductivities of materials were studied with the help of Thermtest thermal conductivity meter, MP-2 with TPS-4. This method is based on the principle of Transient Plane Source Method. A circular disc of diameter 13 mm/25mm and thickness of 3 mm was placed on the flat sensor of the thermtest device, and the thermal conductivity was measured at room temperature.

Structural analysis

The crystal structures have been previously reported for these two materials [6,7]. $Ca_2Fe_2O_{6-\delta}$ is a brownmillerite type compound with tetrahedral layers alternating with octahedral layers as shown in (Figure 1). Each tetrahedral chain in a layer is oriented in the opposite direction of the tetrahedral chain of the other nearest layer (above and below). Thus, the tetrahedral layers are arranged in the alternating orientation as shown in (Figure 1) (inset). It has a space group, *Pnma* [7], (Figure 1) and (Table 1) show the Rietveld refinement profile and parameters of $Ca_2Fe_2O_{6-\delta}$, respectively. There is a structural variation due to difference in the ionic radii of Sr^{2+} and Ca^{2+}. When Ca is completely replaced by Sr, the oxygen vacancy arrangements create different coordination geometry around Fe. In $Sr_2Fe_2O_{6-\delta}$, square pyramids (as shown in (Figure 2) inset) are formed around Fe instead of tetrahedral coordination geometry like in $Ca_2Fe_2O_{6-\delta}$. (Figure 2) and (Table 2) show the Rietveld refinement profile and parameters of $Sr_2Fe_2O_{6-\delta}$, respectively. It has tetragonal crystal structure with I4/mmm space group.

How to cite this article: Ram Krishna H, Amara M, Mandy G , Alexa D A. Study of Thermal Insulation Nature of $A_2Fe_2O_{6-\delta}$ (A and A' = Ca, Sr). Eng Technol Open Acc 2024; 5(5): 555671. DOI: 10.19080/ETOAJ.2024.05.555671

(Figure 3) is the SEM micrographs of $Ca_2Fe_2O_{6-\delta}$ and $Sr_2Fe_2O_{6-\delta}$ that illustrates their microstructure. The SEM images demonstrate the different grain geometries and different grain growth style in these materials which is expected because of the structural variation. However, one common thing is the micro size of the grains in these materials.

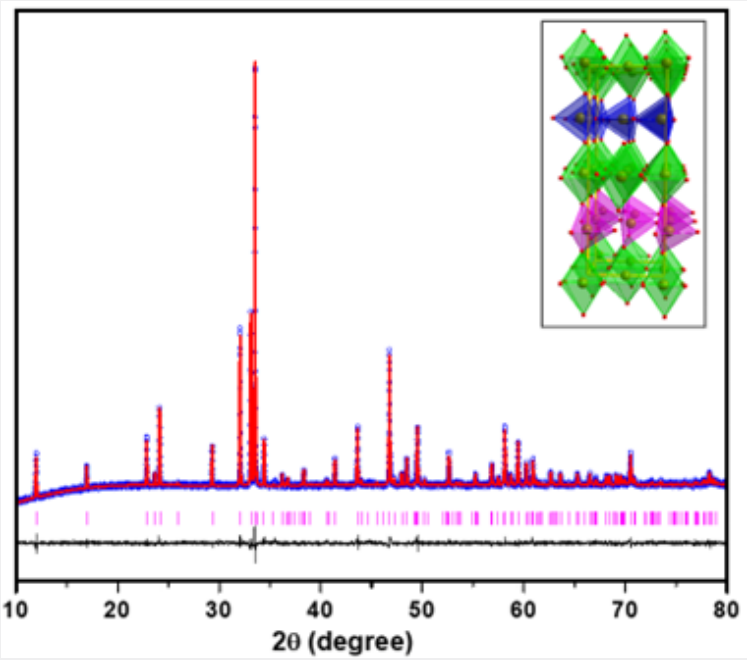

Figure 1: The Rietveld refinement profile of $Ca_2Fe_2O_{6-\delta}$. The blue circles, red line, pink vertical lines, and black solid line represent the raw data, the model, Bragg peak positions, and difference plot, respectively. The inset shows the crystal structure with an orthorhombic unit cell and *Pnma* space group.

Table 1: Rietveld refinement parameters of $Ca_2Fe_2O_{6-\delta}$.

Element	x	y	z	Uiso	Multiplicity	Occupancy
Ca	0.4808(5)	0.1079(2)	0.0247(6)	0.028	8	1
Fe1	0.0000	0.0000	0.0000	0.027(6)	4	1
Fe2	-0.0548(3)	0.2500	-0.0669(9)	0.030(2)	4	1
O1	0.2573(2)	-0.0154	0.2344(2)	0.027(3)	8	1
O2	0.0295(2)	0.1420(3)	0.0774(2)	0.019(1)	8	1
O3	0.6106(7)	0.2500	-0.1250(5)	0.014(2)	4	1

Space group = Pnma, a = 5.4024(1) Å, b = 14.7017(3) Å, c = 5.5726(3) Å, wRp =0.0177, Rp = 0.0132

Both compounds, $Ca_2Fe_2O_{6-\delta}$, and $Sr_2Fe_2O_{6-\delta}$ were prepared by solid-state reaction at high temperatures as described previously [22] The detailed synthesis methods and conditions are described in the supporting information. The crystal structure and phase purity were investigated by Rietveld refinement of powder x-ray diffraction [20,21] The parameters and the profile of the refinements for both compounds are mentioned in supporting information (Tables 1&2). These materials have already been reported for their crystal structures [22] These materials demonstrate different types of oxygen vacancy (oxygen defect) arrangements leading to different coordination geometries and crystal structures.

$Ca_2Fe_2O_{6-\delta}$ possesses tetrahedral layers alternating with octahedral layers giving rise to brownmillerite type structures. This compound has an orthorhombic structure. Note that A-site cation substitutions are made for the two compounds. The substitution of Sr for Ca transforms the crystal structure. In this material, $Ca_2Fe_2O_{6-\delta}$, vacancies form FeO_4 tetrahedra forming chains as mentioned before and running the tetrahedral layer parallel to the layer of FeO_6 octahedra. $Ca_2Fe_2O_{6-\delta}$ has Pnma space group where a layer of tetrahedra is oriented in the direction opposite to the other nearest tetrahedral layers above and below it [9,22,23]. The arrangements of tetrahedral and octahedral layers are illustrated in (Figure 1) for $Ca_2Fe_2O_{6-\delta}$. In $Sr_2Fe_2O_{6-\delta}$, the

How to cite this article: Ram Krishna H, Amara M, Mandy G , Alexa D A. Study of Thermal Insulation Nature of $A_2Fe_2O_{6-\delta}$ (A and A' = Ca, Sr). Eng Technol Open Acc 2024; 5(5): 555671. DOI: 10.19080/ETOAJ.2024.05.555671

vacancies form BO_5 square pyramids [9]. Two square pyramids share oxygen at a corner facing the connected square pyramids opposite to each other. Thus, the two square pyramids have B_2O_9 atoms and form a dimer of opposite faces. The Rietveld refinement parameters and crystal structure of $Sr_2Fe_2O_{6-\delta}$ are given in supporting information. It can be seen in (Figure 2) inset that the B_2O_9 dimers are separated from one another by octahedra. The square pyramids and the octahedra are connected by corner-sharing through oxygens [9] (Figures 1,2&3).

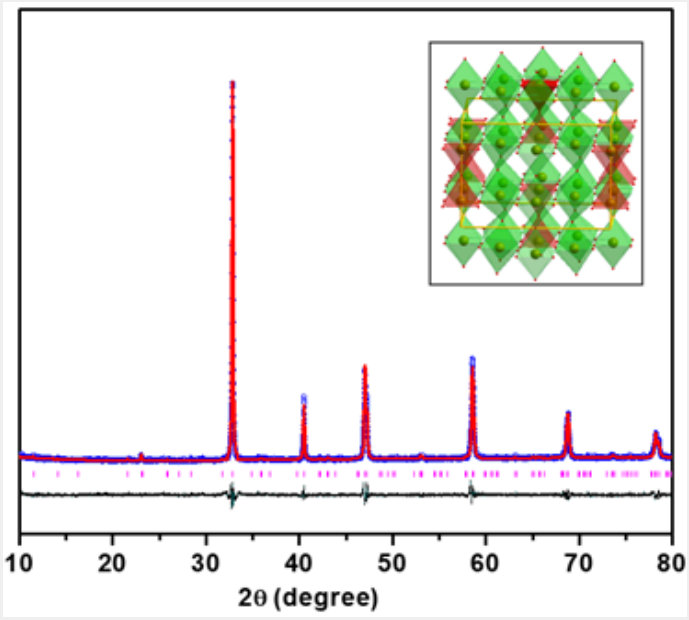

Figure 2: The Rietveld refinement profile of $Sr_2Fe_2O_{6-\delta}$. The blue circles, red lines, pink vertical lines, and black solid lines represent the raw data, the model, Bragg peak positions, and the difference plot, respectively. The inset shows the crystal structure with a tetragonal unit cell and I4/*mmm* space group.

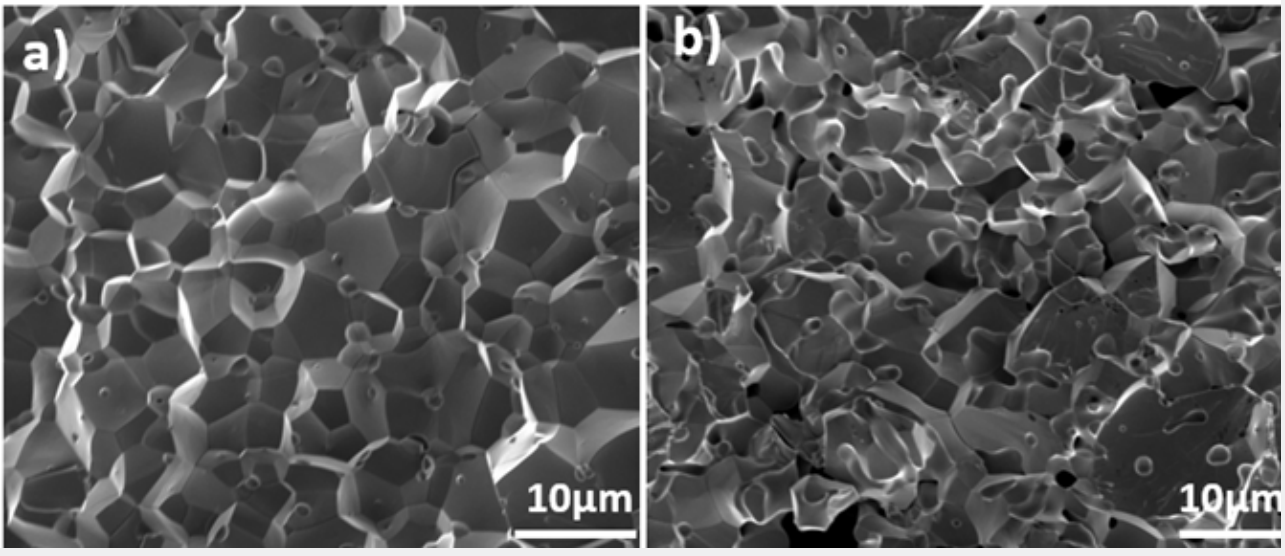

Figure 3: SEM images of a) $Ca_2Fe_2O_{6-\delta}$ b) $Sr_2Fe_2O_{6-\delta}$: the grains look closely packed in them.

How to cite this article: Ram Krishna H, Amara M, Mandy G , Alexa D A. Study of Thermal Insulation Nature of $A_2Fe_2O_{6-\delta}$ (A and A' = Ca, Sr). Eng Technol Open Acc 2024; 5(5): 555671. DOI: 10.19080/ETOAJ.2024.05.555671

Table 2: Rietveld refinement parameters of $Sr_2Fe_2O_{6-\delta}$.

Element	x	y	z	Uiso	Multiplicity	Occupancy
Sr1	0.2601(2)	0.0000	0.0000	0.015(1)	8	1
Sr2	0.2480(1)	0.0000	0.5000	0.014(1)	8	1
Fe1	0.0000	0.0000	0.2500	0.019(6)	4	1
Fe2	0.2500	0.2500	0.2500	0.010(1)	8	1
Fe3	0.5000	0.0000	0.2500	0.032(1)	4	1
O1	0.0000	0.0000	0.2500	0.028(1)	2	1
O2	0.1231(2)	0.1231(2)	0.2241(1)	0.010(1)	16	1
O3	0.2537(7)	0.2537(7)	0.5000	0.014(6)	8	1
O4	0.1253(7)	0.6253(7)	0.2500	0.016(4)	16	1
O5	0.5000	0.0000	0.0000	0.042(2)	4	1

Space group = I4/mmm, a = 10.9343(9) Å, b = 10.9340 Å, c = 7.6988(8) Å, wRp =0.0311, Rp = 0.0216

The lowest thermal conductivity reported for perovskite oxides, as far as I know, is near 1 $Wm^{-1}K^{-1}$ [16]. Recently studied vacancy-ordered material reported the thermal conductivity of ~0.5 Wm-1K-1 showing the relation of vacancy order to the reduced thermal conductivity. Both materials reported here are vacancy ordered, though with different arrangements. Both these materials, $Ca_2Fe_2O_{6-\delta}$, and $Sr_2Fe_2O_{6-\delta}$ exhibit the thermal conductivity of < 1 at room temperature. $Sr_2Fe_2O_{6-\delta}$ has thermal conductivity of ~0.5 which is one among the lowest values reported yet for perovskite oxide materials, so far, we know. (Figure 4) shows the bar diagram for the thermal conductivities of $Ca_2Fe_2O_{6-\delta}$, and $Sr_2Fe_2O_{6-\delta}$ for their comparative study and (Table 3) shows the actual values of the two materials. This value also supports the relation of the vacancy order to the reduced thermal conductivity of the recent report [14]. These materials were synthesized by solid-state reaction at high temperatures in the same way and environment as the other previously reported perovskite oxides [24-26].

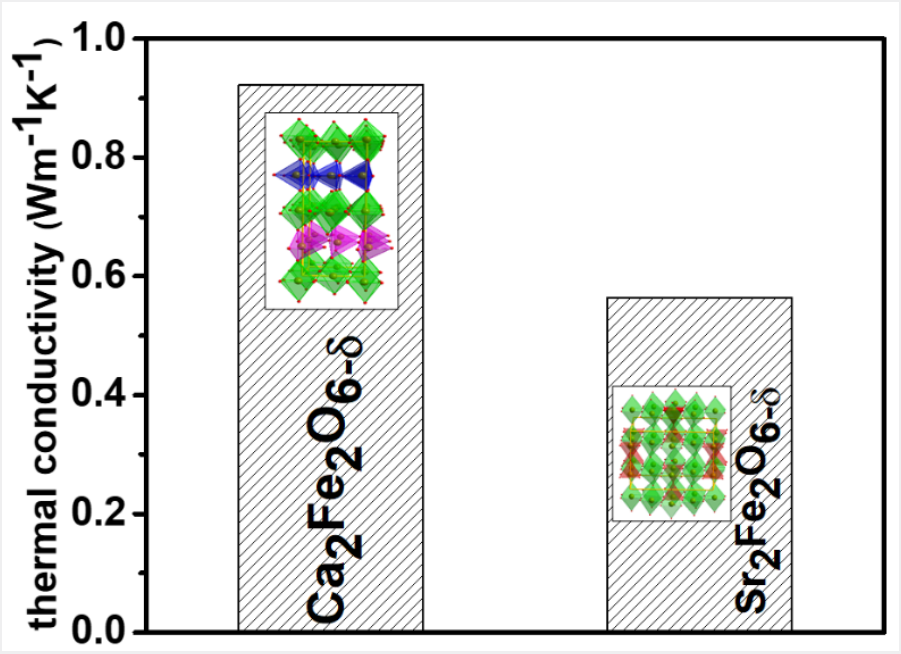

Figure 4: Comparative bar diagram for the thermal conductivities of $Ca_2Fe_2O_{6-\delta}$, and $Sr_2Fe_2O_{6-\delta}$ at room temperature.

How to cite this article: Ram Krishna H, Amara M, Mandy G , Alexa D A. Study of Thermal Insulation Nature of $A_2Fe_2O_{6-\delta}$ (A and A' = Ca, Sr). Eng Technol Open Acc 2024; 5(5): 555671. DOI: 10.19080/ETOAJ.2024.05.555671

Table 3: Thermal conductivity data of $Ca_2Fe_2O_{6-\delta}$, and $Sr_2Fe_2O_{6-\delta}$ at room temperature.

$Ca_2Fe_2O_{6-\delta}$	$Sr_2Fe_2O_{6-\delta}$
0.922 ± 0.098 ($Wm^{-1}K^{-1}$)	0.568 ± 0.095 ($Wm^{-1}K^{-1}$)

Thermal conductivity (K) was assessed by the Thermtest thermal conductivity meter, MP-2 with TPS-4 which is based on the principle of Transient Plane Source Method. It utilizes a plane sensor and a special mathematical model describing the heat conductivity, combined with electronics, and enables the method to be used to measure Thermal Transport Properties [27,28].

We also measured the thermal conductivity of a standard sample, the Pyrex verification sample, to check the reliability of the equipment. It showed a thermal conductivity of pyrex as 1.117 $Wm^{-1}K^{-1}$ which is equal to the value given in the instruction manual and it validates the thermal conductivity data of our materials. As discussed above attempts have been made for the reduction of thermal conductivity in perovskite oxides by A-site or B-site cation substitution [16]. Ca and rare earth elements substitution in A-site in $Sr_{0.9-x}CaxLa_{0.1}TiO_3$ ($0 < x < 0.6$) suppressed the thermal conductivity.16, 29 The thermal conductivity was reported to reduce from 4.7 to 3.3 $Wm^{-1}K^{-1}$ when the value of x increased from 0 to 0.6. Similarly, the thermal conductivity reduction was reported for $La_{1-x}Ba_xCoO_3$ as the value of x increased more and more [15]. Sr was also used in place of Ba to reduce the thermal conductivity in $La_{1-x}Sr_xCoO_3$ where the thermal conductivity decreased with the increase of x value [16,30]. It indicates that Sr and Ba concentrations increase with the value of x in those complexes (in both examples), and so does the oxygen vacancy in the crystal lattice because La (+3 oxidation) is partially substituted by Sr and Ba (+2 oxidation). The defect formation can lead to increased phonon scattering and the suppression of lattice thermal conductivity [15,16,30]. The thermal conductivity reduction can be the result of the reduction of the mean free path of the phonon [16,31]. Thus, the lattice distortion and phonon scattering can be the factors for the thermal conductivity reduction [32,33] Phonon scattering can sometimes be led by B site cation substitution in perovskite oxides. One example of such a study was CaMnO3 where Mn was partially substituted by different elements [16,34-37]. Thus, B site cation can also cause the phonon scattering and suppressing the lattice thermal conductivity.

In our study, A cations have been substituted for the study. The reason behind the lower thermal conductivity of our materials can be analyzed by different aspects as discussed before such as oxygen vacancy, structural transformation, lattice distortion, grain size and boundary, etc. Since our materials show structural transformation due to A cation substitution, the possibility of lattice distortions can be ruled out for the contribution of phonon scattering. SEM images (Figure 3) show clear grains and boundaries indicating the well-sintered materials. Smaller grains scatter phonons more than the bigger ones. Both materials show micrometer-sized grains. The small grain size observed in these materials is important for low lattice thermal conductivity (κ) due to more phonon scattering [38]. Though the grain growth seems to be different in the two materials, the grain size does not seem significantly different. It indicates that the difference in grain size does not have a significant contribution to the thermal conductivity of our materials. Phonon scattering was sometimes realized by the introduction of grain boundaries [16,37]. A report already discussed the effect of grain boundary on thermal conductivity/resistance due to its contribution to phonon scattering [16,37,39] However, both materials show clear grain boundaries but with no significant difference. So, the contribution of the grain boundary can also be ignored. These materials have already been studied extensively for their structures and charge transport properties [9,40] They show different charge transport at room temperature. However, the thermal conductivity difference is not significant for the materials implying the insignificant contributions of charge carriers. There are reports for the insignificant contribution of charge carriers to the thermal conductivity in similar materials [24,25].

In most cases, electrons can be the thermal energy carriers. Hence, Fe^{3+} and Fe^{4+} spins may play a role in thermal conductivity. However, this is not the only factor that controls thermal conductivity. In the case of electron-doped $CaMnO_3$ or $Ca_{0.9}R_{0.1}MnO_3$, the contribution of phonon scattering becomes more dominant over the contributions of electrons and spins [25]. Similarly, a $SrTiO_3$-related oxygen-deficient compound demonstrated the dominant effect of phonon scattering over electronic contribution [24]. The experiment patterns and result patterns of our materials are similar to the previous reports. So, the contribution of the spins can be considered insignificant.

The sum of the contributions from phonons and photons (radiations) gives the total thermal conductivity (K).

$$K = K_p + K_R$$

where K_R represents the thermal conductivity contribution by radiation and K_p represents the thermal conductivity contribution of phonon scattering by grain boundaries, lattice, and point defects [41,42].

As has been discussed before, the thermal conductivity decreases as the phonon scattering increases. The heat flow takes place through a spectrum of phonons with different wavelengths and mean-free paths [12,13]. The interference on thermal phonons slows the propagation of heat [13]. It is well understood that local lattice distortions, structures containing void spaces, random vacancies, etc. can act as the sites for phonon scattering resulting in reduced thermal conductivity. The efforts on PbTe–PbSe and Bi_2Te_3-Sb_2Te_3 films have demonstrated how phonon scattering can lower lattice thermal conductivity [12]. The porous yttria-stabilized zirconia was considered to have the phonon scattering due to (i) oxygen vacancies, and (ii) oxygen vacancy jumping [42]. The oxygen vacancies are expected to suppress the

How to cite this article: Ram Krishna H, Amara M, Mandy G , Alexa D A. Study of Thermal Insulation Nature of $A_2Fe_2O_{6-\delta}$ (A and A' = Ca, Sr). Eng Technol Open Acc 2024; 5(5): 555671. DOI: 10.19080/ETOAJ.2024.05.555671

thermal conductivity due to the phonon scattering [43]. The low thermal conductivity of our materials must also be ascribed to suppression of lattice thermal conductivity and increased phonon scattering due to oxygen vacancies [29,30,33,44]. It indicates that the oxygen vacancy plays a role in lowering thermal conductivity. The suppression of thermal conductivity by the introduction of a small amount of oxygen vacancy has already been reported [16,43] We already discussed the experiments and calculations of oxygen vacancy (δ) for these compounds in the previous report [9,23] The δ values for $Sr_2Fe_2O_{6-\delta}$ is 0.25, and $Ca_2Fe_2O_{6-\delta}$ is 1.0.

Overall, oxygen vacancies play an essential role in increasing the phonon scattering and lowering thermal conductivity in our materials. Phonon scattering becomes disproportionately dominant over contributions of other factors discussed above (grain size, boundary, and spins) for thermal wave propagation [24,25] is dominant. Since phonon scattering is importantly considered to be responsible for lowering thermal conductivity in the above discussions, the low thermal conductivity of our compounds is due to oxygen vacancy. Again, the thermal conductivity of the compounds $Sr_2Fe_2O_{6-\delta}$ (δ =0.25) is lower than that of $Ca_2Fe_2O_{6-\delta}$ (δ =1). This implies that the vacancy ordering may have contributed to this thermal conductivity difference.

Conclusion

Two oxygen-deficient perovskite oxides ($Ca_2Fe_2O_{6-\delta}$ and $Sr_2Fe_2O_{6-\delta}$) are being investigated for their thermal insulation property. Though these compounds have different oxygen vacancy arrangements, they, both, are vacancy ordered. These materials, $Ca_2Fe_2O_{6-\delta}$ shows the thermal conductivity of ~0.9 $Wm^{-1}K^{-1}$ and $Sr_2Fe_2O_{6-\delta}$ demonstrated ~0.5 $Wm^{-1}K^{-1}$. Thus, $Sr_2Fe_2O_{6-\delta}$ has better thermal insulating properties with the low thermal conductivity of ~0.5 $Wm^{-1}K^{-1}$ which is one among the lower thermal conductivity of reported perovskite oxides. The main contributing factors for lowering the thermal conductivity of these compounds are phonon scattering due to oxygen vacancies and their ordered arrangements.

Funding: Instructional Capacity Excellence in TCUP Institutions (ICE-TI) award # 1561004 and NSF Tribal Enterprise Advancement Center award grant no. HRD 1839895.

Institutional Review Board Statement: Not Applicable.

Informed Consent Statement: Not applicable.

Acknowledgments: This work is supported in part by the National Science Foundation Tribal College and University Program Instructional Capacity Excellence in TCUP Institutions (ICE-TI) award # 1561004. A part of this work is also supported by NSF grant no. HRD 1839895. Additional support for the work came from ND EPSCOR STEM grants for the purchase of a potentiostat and X-ray diffractometer and the American Indian College Fund for the thermal conductivity meter. The views expressed are those of the authors and do not necessarily represent those of United Tribes Technical College.

Conflicts of Interest: The authors declare no conflict of interest.

References

1. Guo Y, Feng S, Yang Y, Zheng R, Zhang Y, et al. (2022) High-entropy titanate pyrochlore as newly low-thermal conductivity ceramics. J Eur Ceram Soc 42(14): 6614-6623.
2. Lee H, Yang S, Wi S, Kim S (2019) Thermal transfer behavior of biochar-natural inorganic clay composite for building envelope insulation. Constr Build Mater 223: 668-678.
3. Liu D, Zhou Z, Wang Y, Xu B (2022) Highly porous (La1/5Nd1/5Sm1/5Gd1/5Yb1/5)2Zr2O7 ceramics with ultra-low thermal conductivity. Ceram Int 48(18): 26400-26407.
4. Wu T, Gao P (2018) Development of Perovskite-Type Materials for Thermoelectric Application. Materials 11(6).
5. Tang S, Wu M, Bai S, Luo D, Zhang J, et al. (2022) Honeycomb-like puckered PbTe monolayer: A promising n-type thermoelectric material with ultralow lattice thermal conductivity. J Alloys Compd 907: 164439.
6. Xu W, Shang PP, Marcelli A, Cibin G, Li, JF (2022) Multiple emerging nano-phases are at the origin of the low lattice thermal conductivity of SnSe? Mater. Today Phys 24: 100656.
7. Liu Q, Liu KF, Wang QQ, Liu XC, Yu F, et al. (2022) Rattling-like scattering behavior in ALiSb (A = Ca, Sr, Eu, Yb) Zintl phases with low thermal conductivity. Acta Mater 230: 117853.
8. Liu Y, Zhang J, Ren G, Chernatynskiy A (2022) Utilizing twin interfaces to reduce lattice thermal conductivity of superlattice. Int J Heat Mass Transf 189: 122700.
9. Hona RK, Huq A, Mulmi S, Ramezanipour F (2017) Transformation of Structure, Electrical Conductivity, and Magnetism in AA′Fe2O6−δ, A = Sr, Ca and A′ = Sr. Inorg Chem 56(16): 9716-9724.
10. Kim J, Yin X, Tsao KC, Fang S, Yang H (2014) $Ca_2Mn_2O_5$ as Oxygen-Deficient Perovskite Electrocatalyst for Oxygen Evolution Reaction. J Am Chem Soc 136(42): 14646-14649.
11. Hona RK, Ramezanipour F (2020) Effect of the Oxygen Vacancies and Structural Order on the Oxygen Evolution Activity: A Case Study of SrMnO3−δ Featuring Four Different Structure Types. Inorg Chem 59(7): 4685-4692.
12. Snyder GJ, Toberer ES (2008) Complex thermoelectric materials. Nat Mater 7(2): 105-114.
13. Maire J, Anufriev R, Yanagisawa R, Ramiere A, Volz S, et al. (2017) Heat conduction tuning by wave nature of phonons. Sci Adv 3(8): e1700027.
14. Hona RK, Karki SB, Dhaliwal G, Guinn M, Ramezanipour F (2022) High Thermal Insulation Properties of A2FeCoO6-δ (A = Ca, Sr). J Mater Chem C 10: 12569-12573.
15. Kun R, Populoh S, Karvonen L, Gumbert J, Weidenkaff A, et al. (2013) Structural and thermoelectric characterization of Ba substituted LaCoO3 perovskite-type materials obtained by polymerized gel combustion method. J Alloys Compd 579: 147-155.
16. Wu T, Gao P (2018) Development of Perovskite-Type Materials for Thermoelectric Application. Materials 11(6): 999.
17. Chen L, Zhang Y, Wang X, Jalan B, Chen S, et al. (2018) Roles of Point Defects in Thermal Transport in Perovskite Barium Stannate. J Phys Chem 122 (21): 11482-11490.
18. Luckyanova MN, Chen D, Ma W, Tuller HL, Chen G, et al. (2014) Thermal conductivity control by oxygen defect concentration modification in reducible oxides: The case of Pr0.1Ce0.9O2-δ thin films. Appl Phys Lett 104(6): 061911.

How to cite this article: Ram Krishna H, Amara M, Mandy G , Alexa D A. Study of Thermal Insulation Nature of $A_2Fe_2O_{6-\delta}$ (A and A' = Ca, Sr). Eng Technol Open Acc 2024; 5(5): 555671. DOI: 10.19080/ETOAJ.2024.05.555671

19. Hofmeister AM (2010) Thermal diffusivity of oxide perovskite compounds at elevated temperature. J Appl Phys 107(10): 103532.

20. Larson AC, Von Dreele RB (1994) General Structure Analysis System (GSAS), Los Alamos National Laboratory Report LAUR 86-748. [20]

21. Toby BH (2001) J Appl Crystallogr 34: 210-213.

22. Hona RK, Huq A, Ramezanipour F (2017) Unraveling the Role of Structural Order in the Transformation of Electrical Conductivity in Ca2FeCoO6−δ, CaSrFeCoO6−δ, and Sr2FeCoO6−δ. Inorg Chem 56(23): 14494-14505.

23. Hona RK, Ramezanipour F (2019) Remarkable Oxygen-Evolution Activity of a Perovskite Oxide from the Ca2−xSrxFe2O6−δ Series. Angew Chem Int Ed Engl 58(7): 2060-2063.

24. Rahman JU, Nam WH, Van Du N, Rahman G, Rahman AU, et al. (2019) Oxygen vacancy revived phonon-glass electron-crystal in SrTiO3. J Eur Ceram Soc 39(2): 358-365.

25. Wang Y, Sui Y, Wang X, Su W, Liu X, et al. (2010) Thermal conductivity of electron-doped CaMnO3 perovskites: Local lattice distortions and optical phonon thermal excitation. Acta Materialia 58(19): 6306-6316.

26. Hona RK, Huq A, Ramezanipour F (2017) Unraveling the Role of Structural Order in the Transformation of Electrical Conductivity in Ca2FeCoO6−δ, CaSrFeCoO6−δ, and Sr2FeCoO6−δ. Inorg Chem 56(23): 14494-14505.

27. Gustafsson SE (1991) Transient plane source techniques for thermal conductivity and thermal diffusivity measurements of solid materials. Rev Sci Instru 62(3): 797-804.

28. Gustavsson M, Karawacki E, Gustafsson SE (1994) Thermal conductivity, thermal diffusivity, and specific heat of thin samples from transient measurements with hot disk sensors. Rev. Sci. Instru. 1994, 65(12): 3856-3859.

29. Muta H, Ieda A, Kurosaki K, Yamanaka S (2004) Substitution effect on the thermoelectric properties of alkaline earth titanate. Mater Lett 58(30): 3868-3871.

30. Berggold K, Kriener M, Zobel C, Reichl A, Reuther M, et al. (2005) Thermal conductivity, thermopower, and figure of merit of La1-xSrxCoO3. Phys Rev B 72(15): 155116.

31. Muta H, Kurosaki K, Yamanaka S (2005) Thermoelectric properties of reduced and La-doped single-crystalline SrTiO3. J Alloys Compd 392(1): 306-309.

32. Kato K, Yamamoto M, Ohta S, Muta H, Kurosaki K, et al. (2007) The effect of Eu substitution on thermoelectric properties of SrTi0.8Nb0.2O3. J Appl Phys 102(11): 116107.

33. Muta H, Kurosaki K, Yamanaka S (2003) Thermoelectric properties of rare earth doped SrTiO3. J Alloys Compounds 350(1): 292-295.

34. Cong BT, Tsuji T, Thao PX, Thanh PQ, Yamamura Y (2004) High-temperature thermoelectric properties of Ca1-xPrxMnO3−δ (0⩽x<1). Phys B Condens Matter 352(1): 18-23.

35. Flahaut D, Mihara T, Funahashi R, Nabeshima N, Lee K, et al. (2006) Thermoelectrical properties of A-site substituted Ca1-xRexMnO3 system. J Appl Phys 100(8): 084911.

36. Maignan A, Martin C, Autret C, Hervieu M, Raveau B, Hejtmanek J (2002) Structural–magnetic phase diagram of Mo-substituted CaMnO3: consequences for thermoelectric power properties. J Mater Chem 12(6): 1806-1811.

37. Bocher L, Aguirre MH, Logvinovich D, Shkabko A, Robert R, et al. (2008) CaMn1-x NbxO3 (x ≤ 0.08) Perovskite-Type Phases as Promising New High-Temperature n-Type Thermoelectric Materials. Inorg Chem 47(18): 8077-8085.

38. Saxena M, Tanwar K. Maiti T (2017) Environmentally friendly Sr2TiMoO6 double perovskite for high temperature thermoelectric applications. Scr Mater 130: 205-209.

39. Feng X, Fan Y, Nomura N, Kikuchi K, Wang L, et al. (2017) Graphene promoted oxygen vacancies in perovskite for enhanced thermoelectric properties. Carbon 112: 169-176.

40. Hona RK, Dhaliwal GS, Thapa R (2022) Investigation of Grain, Grain Boundary, and Interface Contributions on the Impedance of Ca2Fe2O5. Appl Sci12 (6).

41. klemens PG (1969) In "Thermal Conductivity," Vol 1, edited by RP Tyne. Academic Press, London, UK, p. 1.

42. Schlichting KW, Padture NP, Klemens PG (2001) Thermal conductivity of dense and porous yttria-stabilized zirconia. J Materials Sci 36(12): 3003-3010.

43. Lee S, Yang G, Wilke RHT, Trolier-McKinstry S, Randall CA (2009) Thermopower in highly reduced n-type ferroelectric and related perovskite oxides and the role of heterogeneous non stoichiometry. Phys Rev B 79(13): 134110.

44. Okuda T, Hata H, Eto T, Nishina K, Kuwahara H, et al. (2014) In Effects of Mn substitution on the thermoelectric properties of the electron-doped perovskite Sr1-xLaxTiO3. J Phys Confer Ser 2014: 022035.

DOI: 10.19080/ETOAJ.2024.05.555671

How to cite this article: Ram Krishna H, Amara M, Mandy G , Alexa D A. Study of Thermal Insulation Nature of $A_2Fe_2O_{6-\delta}$ (A and A' = Ca, Sr). Eng Technol Open Acc 2024; 5(5): 555671. DOI: 10.19080/ETOAJ.2024.05.555671